T. Wintergerste & L. Kleiser

Direct Numerical Simulation of Transition in a Three-Dimensional Boundary Layer

Abstract

Transition to turbulence in a three-dimensional boundary layer is investigated by a highly resolved direct numerical simulation adapted to a transition experiment made at DLR Göttingen. A parallel base flow is defined locally by Falkner-Skan-Cooke similarity profiles. As shown earlier, the temporal simulation results can be related to the spatial disturbance development in the experiment and show good agreement with measurements. The crossflow vortices, which develop as a primary instability of the laminar flow, break down at the late stages of the transition process. At the end of transition, the shape factor and local skin friction coefficient of the computed mean velocity profile reach their turbulent levels. Particular attention is given to the development of flow structures in the breakdown stage. A new three-dimensional vortical structure is found to emerge which propagates with approximately 70% of the free-stream velocity in the streamwise direction. Vortical structures are identified by different criteria based on local pressure minima or the velocity-gradient tensor ∇u.

Introduction

Transition to turbulence in the swept wing boundary layer of a modern aircraft can be caused by different instability mechanisms. The crossflow instability dominates regions on the wing where a strong favourable pressure gradient exists. This instability is characterized by the presence of co-rotating stationary crossflow vortices and travelling waves which are both linearly unstable. For an overview readers are referred to the paper by Reed & Saric (1989).

Experiments and theoretical investigations have shown that nonlinear interactions play an important role already at early stages of the transition process. These stages are characterized by interactions between the crossflow vortices and the travelling waves. At the highly nonlinear stages of transition, a secondary instability with a frequency a magnitude larger than the travelling primary disturbances was observed in the experiments by Kohama *et al.* (1991). This instability was also observed in theoretical investigations by Malik *et al.* (1994) based on PSE in a swept Hiemenz flow. They found that the high-frequency instability is associated with a shear layer on the upper side of the crossflow vortex. The processes at the late stages which lead to the breakdown of the crossflow vortex and to the onset of turbulence are not yet fully understood.

Our investigations are adapted to the transition experiment by Bippes *et al.* (1991). Various attempts have been made at clarifying the transition process

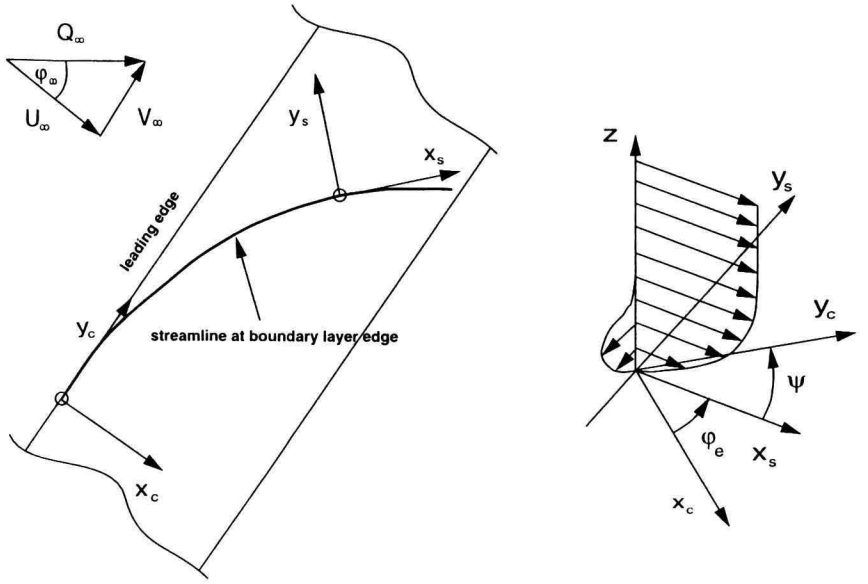

Figure 1: Sketch of the DLR swept plate transition experiment (Bippes *et al.*, 1991).

observed in this experiment. Fischer & Dallmann (1992) find a good agreement between the results of the secondary stability of the crossflow-vortex modulated base flow and the experiment. Meyer and Kleiser (1989,1990) and Wagner (1992) carried out temporal simulations of the 3D-boundary layer transition. They observed a strong deformation of the mean flow which agrees well with the experimental observations. These simulations reached a highly developed stage of transition but they were not fully resolved in the late breakdown stage of the crossflow vortices.

In this contribution we present a continuation of the latter work which includes the complete breakdown process. Our interest will be focussed on the flow phenomena occurring in the late stages of transition where the crossflow vortices break down and the boundary layer becomes turbulent.

Base flow

The simulation presented here is adapted to the DLR transition experiment (Bippes *et al.*, 1991) in which a three-dimensional boundary layer develops on a swept flat plate. A displacement body above the plate is used to generate an approximately constant negative pressure gradient normal to the leading edge. A sketch of the various coordinate systems which are used is given in Fig. 1. The coordinate system aligned with the local streamline direction is denoted by (x_s, y_s). In the vortex-oriented system the coordinate x_v points into the direction of the crossflow vortex axis, which is determined from linear stability analysis. It

includes a small angle ϵ with the x_s direction. The angle ϵ is determined by linear stability analysis as the angle between the local streamline and the most amplified primary disturbance, i.e. the crossflow. The simulations have been carried out in the vortex-oriented system. The wall-normal direction is denoted by z. All quantities are nondimensionalized by the reference length $\tilde{d} = [(\tilde{\nu}\tilde{x}_c)/\tilde{U}_{0c,e}]^{1/2}$ (where $\tilde{\nu}$ is the kinematic viscosity and an index "0" refers to the undisturbed laminar base flow) and the magnitude of the local velocity at the boundary layer edge $\tilde{Q}_{0,e}$. The local Reynolds number is defined by $Re = (\tilde{Q}_{0,e}\tilde{d})/\tilde{\nu}$.

The boundary layer can be approximated locally by Falkner-Skan-Cooke (FSC) similarity solutions (Cooke, 1950) as demonstrated by Meyer & Kleiser (1989). The profiles depend on the local sweep angle φ_e and the Hartree parameter β_h. These parameters are taken from the experiment. Our computation simulates the development of the disturbances in the rearward region of the plate. In this region the two parameters φ_e and β_h are nearly constant. We have chosen a position of 80% chord-length of the plate. Under the conditions of the experiment, this results in a local Reynolds number of $Re = 826$, a sweep angle of $\varphi_e = 46.9^o$ and a Hartree parameter of $\beta_h = 0.63$.

Numerical method

The nonlinear development of the streamwise and spanwise periodic disturbances is computed by solving the three-dimensional incompressible time-dependent Navier-Stokes equations. A Fourier/Chebychev spectral method is used for the spatial discretization. For the time integration a four-stage third-order Runge-Kutta scheme is employed for the nonlinear terms and an implicit Crank-Nicolson scheme for the viscous terms. The nonlinear term is computed aliasing-free in the wall-parallel directions. Earlier simulations by Meyer & Kleiser (1989) and Wagner (1992) showed that the results of the temporal simulation are in good agreement with the experimental results at corresponding stages of the development.

Results

In the present investigations we are mainly interested in the processes occurring in the highly nonlinear stages of transition, when the stationary crossflow vortex breaks down and the flow becomes turbulent. The spatial discretization of the computational domain has been increased up to $N_x \cdot N_y \cdot N_z = 240 \cdot 192 \cdot 160$ grid points. This number is increased by a factor of 3/2 in the wall-parallel directions for the alias-free calculation of the nonlinear terms.

The streamwise and spanwise wave numbers are chosen as $\alpha_v = 0.08$ and $\beta_v = 0.48$. The computational domain captures one crossflow vortex in the spanwise direction. The streamwise length of the domain is chosen from secondary stability theory. The initially excited travelling disturbance with the streamwise wavenumber α_v and spanwise wavenumber β_v gives the maximum

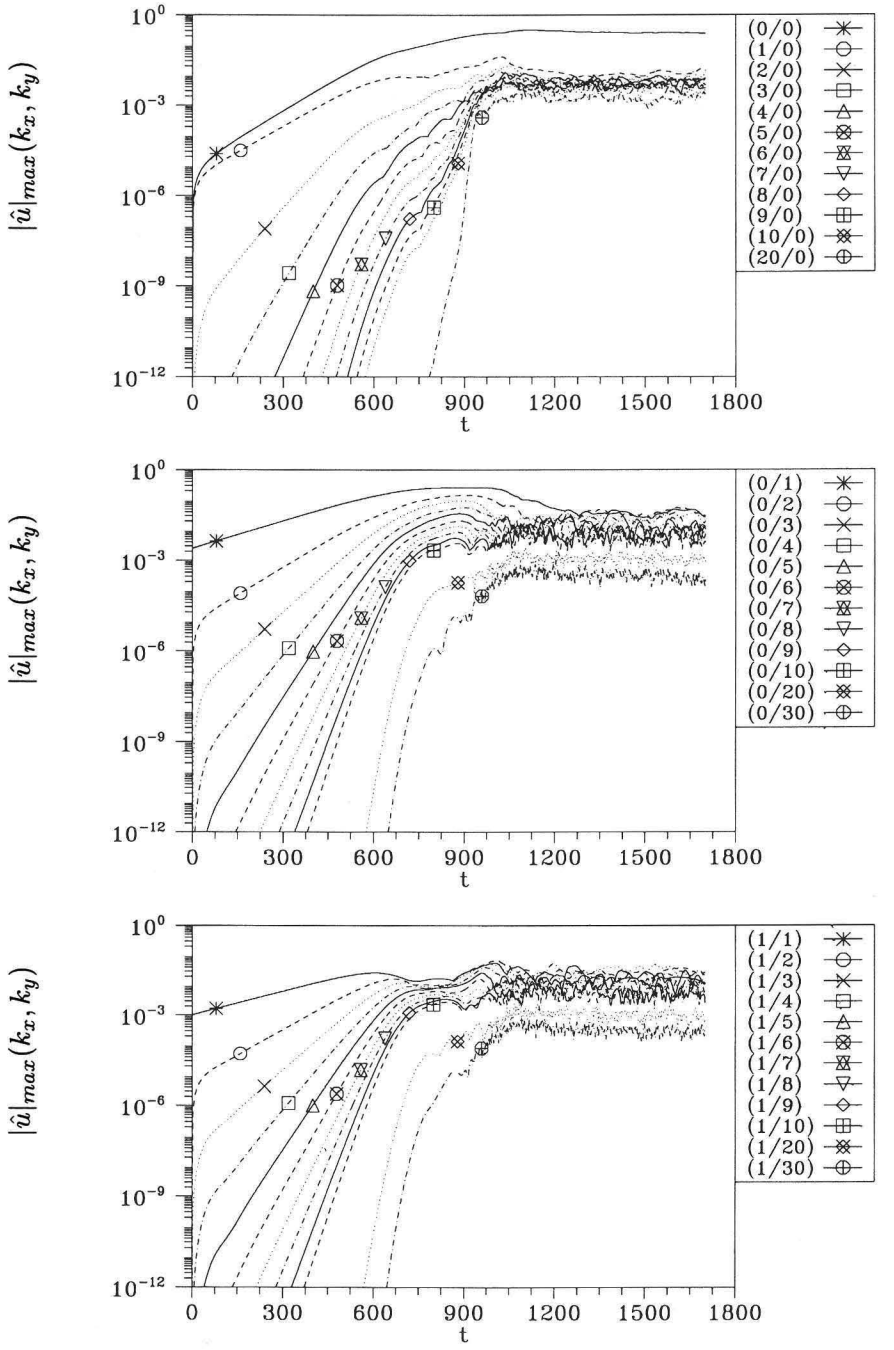

Figure 2: Development of the maximum in the wall-normal direction of the Fourier amplitudes $|\hat{u}|(k_x, k_y)$.

secondary amplification rate as predicted by the secondary stability theory (Fischer & Dallmann, 1992). As initial disturbances a crossflow vortex with an amplitude of $A_{CF} = 0.25\%$ of the free-stream velocity U_v and a travelling three-dimensional disturbance with an amplitude of $A_{tr} = 0.1\%$ were superimposed. The temporal development of the maximum in the wall-normal direction of the Fourier-amplitudes $|\hat{u}|(k_x, k_y)$ is shown in Fig. 2. Both initial modes grow exponentially up to the time $t \approx 600$ as predicted by the linear stability theory. The higher harmonic modes are generated in a regular cascade by the nonlinearity of the Navier-Stokes equations. Between time $t \approx 700$ and $t \approx 920$ the longitudinal vortex modes $\hat{u}(0, k_y)$ reach an approximate saturation, while the travelling wave modes $\hat{u}(k_x, 0)$ are still growing. The maximum of the amplitude of the crossflow vortex reaches a value of $A_{CF} \approx 13\%$ and the amplitude of the travelling wave $A_{tr} \approx 3\%$. Beyond the time $t \approx 920$ the maxima of the Fourier modes are highly fluctuating, and the boundary layer becomes turbulent.

Viewed in streamwise direction, the crossflow vortex rotates in counter-clockwise direction. Thus, the vortex moves slow fluid from the lower part to the upper part of the boundary layer and generates layers of high shear $\partial u/\partial y$ and $\partial u/\partial z$. Faster fluid from the upper part of the boundary layer moves closer to the wall. Velocity profiles with two inflection points can be obtained due to the upward motion of the slow fluid.

Fig. 3b shows the vortical structures identified by the same criterion at a later time $t = 920$. In addition to the crossflow vortex, a new three-dimensional structure is formed in the downstream part of the domain. The foot-print of this new structure can also be found in the wall-pressure distribution, where it marks a strong minimum. Downstream of the three-dimensional vortex a region of high pressure fluctuations is observed. The identification of this flow structure as a vortex can also be confirmed by calculating streamlines in a moving frame of reference. This vortex, which generates new shear layers, moves downstream rapidly and initiates the local breakdown of the crossflow vortex. The visualization of the flow fields at later times shows that the breakdown spreads from this new vortex while in the remaining part of the flow the saturated crossflow vortex persists (Fig. 3c). When the spreading has covered the full domain the entire flow field becomes turbulent (Fig. 3d).

The identification of vortical structures by isosurfaces of low static pressure can only capture vortices with the largest pressure minimum. This criterion fails if vortical structures with different strength appear in the flow. In Fig. 4 the identification of vortical structures by a "*second eigenvalue criterion*" is shown at two earlier times in order to investigate the emergence of the new structure mentioned above. This criterion, which is based on the velocity gradient tensor ∇u, was first used by Jeong & Hussain (1995). It can also be interpreted as locating the "inflection points" of the pressure field, and it allows to determine vortices with different core pressure minima.

Next, the breakdown of the crossflow vortex and the onset of turbulence is investigated by visualizations of the vortical structures which appear in the flow. These structures are important for the energy transfer from the large

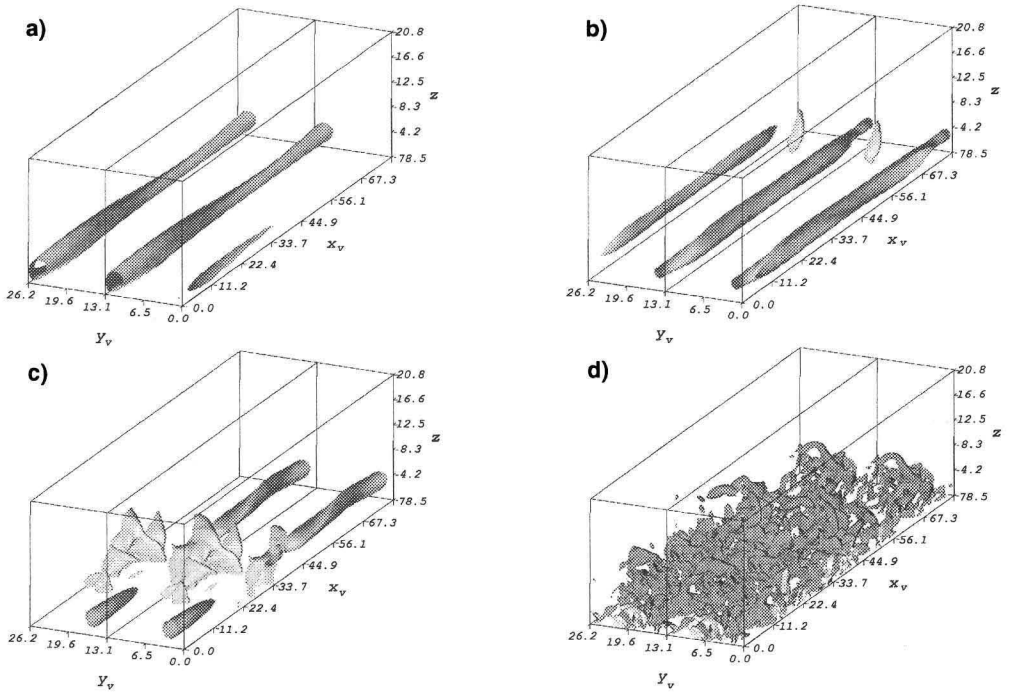

Figure 3: Visualization of vortical structures by isosurfaces of low static pressure. For visualization twice the computational domain in the spanwise direction y is shown. a): $t = 800$, $p_{iso} = -0.0022$; b): $t = 920$, $p_{iso} = -0.0031$; c): $t = 970$, $p_{iso} = -0.004$; d): $t = 1300$, $p_{iso} = -0.005$.

scales to the smaller ones. Different criteria for their identification can be applied to the three-dimensional flow field (e.g. Wintergerste *et al.*, 1995). In Fig. 3a the crossflow vortex is visualized by the most common criterion - isosurfaces of low static pressure - at time $t = 800$ where a near-saturation state of the crossflow vortex is obtained. The modulation in the x_v-direction is caused by the imposed travelling wave.

Fig. 4 shows that a second near-wall streamwise vortex next to each crossflow vortex has been generated at time $t = 800$. This secondary vortex is much weaker than the crossflow vortex. While the centre of the crossflow vortex is located at a height of 50% of the laminar boundary layer thickness δ this vortex is located at a height of approximately $0.15\,\delta$. The new vortex is induced by the co-rotating crossflow vortices in the presence of the wall and rotates in clockwise direction, that is opposite to the rotation direction of the main vortex. Such a near-wall streamwise vortex was also found by Malik *et al.* (1994) in their simulation of swept Hiemenz flow. At time $t = 850$ it moves to the upper side of the crossflow vortex. The interaction of these two vortical structures with the travelling wave which has grown to finite amplitude then leads to the three-dimensional vortical

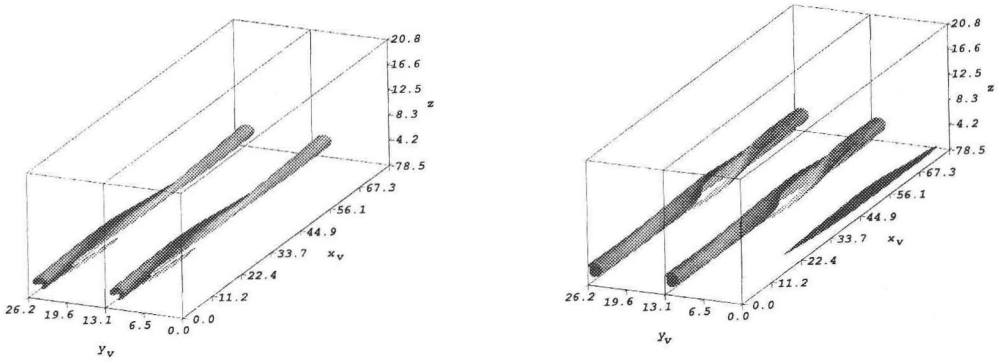

Figure 4: Visualization of the vortical structures by the second eigenvalue criterion. Left: Time $t = 800$; Right: Time $t = 850$. The isovalue is set to -0.001.

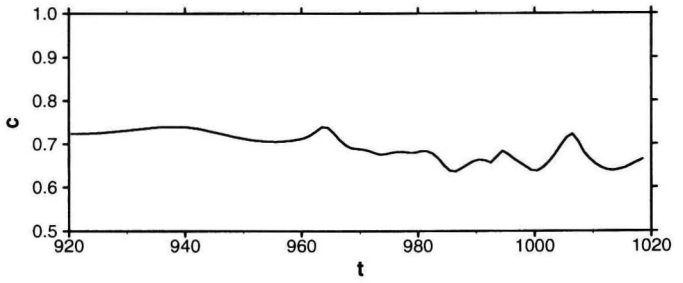

Figure 5: Propagation velocity of the new three-dimensional vortical structure from time $t = 920$ to $t = 1020$.

structure which was visualized in Fig. 3 by isosurfaces of low static pressure. This structure moves to the upper part of the crossflow vortex with increasing time. As mentioned above, a foot-print of this structure can be found in the wall-pressure distribution already at early times of its appearance.

In order to estimate the propagation velocity of the new three-dimensional vortical structure, we consider the correlation of the wall-pressure distribution at two time steps t and $t + \tau$ given by

$$R(\tau, \Delta l)|_{(t,l)} = \frac{\overline{p_{wall}(t,l) \cdot p_{wall}(t+\tau, l+\Delta l)}}{\sqrt{\overline{p_{wall}(t,l)^2} \cdot \overline{p_{wall}(t+\tau, l+\Delta l)^2}}}. \tag{1}$$

Here $p_{wall}(t,l)$ is the wall-pressure fluctuation in a $(x,y)-$window which encloses the foot-print of the vortex, whose streamwise position is denoted as l. Averages are taken over the window. From the shift of the maximum of the correlation function the propagation velocity of the vortical structure can be estimated. In Fig. 5 the propagation velocity of the three-dimensional vortical structure

from time $t = 920$ to $t = 1020$ is shown. One can see that the propagation velocity is approximately 70% of the free-stream velocity. This velocity is an order of magnitude larger than the phase velocities of the most-amplified primary travelling waves.

Conclusions

The complete transition process in a three-dimensional boundary layer has been simulated using the temporal model. After the crossflow vortices, which are excited as primary disturbances, have grown to finite amplitude, small secondary streamwise vortices appear close to the wall next to each crossflow vortex. The breakdown of the crossflow vortices appears to originate from the interaction of these vortices with finite-amplitude travelling waves. From this interaction new three-dimensional vortices emerge which locally initiate the final breakdown of the crossflow vortices. The three-dimensional vortices move downstream with a propagation velocity of approximately 70% of the free-stream velocity, which is an order of magnitude larger than the phase velocity of the initially excited travelling wave. This local breakdown finally spreads over the entire domain and makes the flow turbulent.

References

Bippes, H., Müller, B. & Wagner, M. 1991 – Measurements and stability calculations of the disturbance growth in an unstable three-dimensional boundary layer. *Physics of Fluids A* **3**, 2371-2377.

Cooke, J.C.,1950 – The boundary layer of a class of infinite yawed cylinders. *Proc. Cambridge Phil. Soc.* **46**, 645-648.

Fischer, T.M. & Dallmann, U. 1992 – Primary and secondary stability analysis of a three-dimensional boundary-layer flow. *Physics of Fluids A* **3**, 2378-2391.

Jeong, J. & Hussain, F. 1995 – On the identification of a vortex. *Journal of Fluid Mechanics* **285**, 69-94.

Kleiser, L. & Zang, T.A. 1991 – Numerical simulation of transition in wall-bounded shear flows. *Annual Review of Fluid Mechanics* **23**, 495-537.

Kohama, Y., Saric, W.S. & Hoos, J.A. 1991 – A high frequency secondary instability of crossflow vortices that leads to transition. In: *Proc. of Boundary Layer Transition and Control Conference*, The Royal Aeronautical Society, Cambridge UK, 4.1-4.13.

Malik, M.R., Li, F. & Chang, C.-L. 1994 – Crossflow disturbances in three-dimensional boundary layers: non-linear development, wave interaction and secondary instability. *Journal of Fluid Mechanics* **268**, 1-36.

Meyer, F. & Kleiser, L. 1989 – Numerical investigation of transition in 3D boundary layers. In: *AGARD-CP-438*, 16-1-16-17.

Meyer, F. & Kleiser, L. 1990 – Numerical simulation of transition due to cross-flow instability. In: *Proc. of Third IUTAM Symposium on Laminar-Turbulent Transition*, Editors: D. Arnal and R. Michel, Springer Verlag, 609-619.

Reed, H.L. & Saric, W.S. 1989 – Stability of three-dimensional boundary layers. *Annual Review of Fluid Mechanics* **21**, 235-284.

Wagner, M. 1992 – Numerische Untersuchungen zum laminar-turbulenten Übergang in zwei- und dreidimensionalen Grenzschichten, *Doct. Dissertation, Universität Karlsruhe, Report DLR-FB 92-36.*

Wintergerste, T., Wilhelm, D. & Kleiser, L., 1995 – Visualization of time-dependent three-dimensional transitional and turbulent flow fields. In: *Visualization Methods in High Performance Computing and Flow Simulation. Proceedings of the International Workshop on Visualization, Paderborn Jan. 18-21, 1994*, Editors: W. Borchers, G. Domick, D. Kröner, R. Rautmann and D. Saupe, International Science Publishers.

Authors' address

Swiss Federal Institute of Technology
Institute of Fluid Dynamics
ETH Zentrum
CH-8092 Zürich, Switzerland